Efficient collinear fourth-harmonic generation by two-channel multistep cascading in a single two-dimensional nonlinear photonic crystal

Martijn de Sterke

School of Physics, University of Sydney, Sydney, NSW 2006, Australia

Solomon M. Saltiel

Faculty of Physics, University of Sofia, 5 J. Bourchier Boulevard, Sofia 1164, Bulgaria

Yuri S. Kivshar

Nonlinear Physics Group, Research School of Physics Sciences and Engineering, Australian National University, Canberra, ACT 0200, Australia

Received November 28, 2000

We investigate efficient fourth-harmonic generation in a single two-dimensional (2D) quadratically nonlinear photonic crystal. We propose a novel parametric process that starts with phase-matched generation of a pair of symmetric second-harmonic waves, which then interact to produce a fourth-harmonic wave that is collinear to the fundamental. We show that this process is more efficient than conventional fourth-harmonic-generation schemes by a factor that reaches 4 at low intensities and discuss how to design and optimize the nonlinear 2D photonic crystals that are implemented in $LiNbO_3$ and $LiTaO_3$. © 2001 Optical Society of America

OCIS codes: 190.0190, 190.2620, 190.4390, 190.4410, 230.0230, 230.4320.

Photonic crystals (or photonic bandgap materials) have attracted much interest lately because of their unique properties and many potential applications in optics.[1] Studies of such materials usually focus on linear wave propagation, which is strongly modified by the photonic bandgaps that appear as a consequence of the periodically varying refractive index. Structures with a constant linear refractive index but a periodically modulated nonlinear quadratic [or $\chi^{(2)}$] response were proposed by Berger[2] and studied experimentally by Broderick *et al.*[3] as a two-dimensional generalization of conventional quasi-phase-matched (QPM) structures. Such structures, referred to here as two-dimensional nonlinear photonic crystals (2DNPC's), have no linear bandgap because of their uniform linear properties, but they can be used for generation of several optical frequencies[3,4] and for frequency transformation.[5] However, the frequency-conversion schemes in 2DNPC that have been considered thus far lead to noncollinear harmonic generation, which considerably detracts from their practical use. In this Letter we demonstrate how to exploit the unique properties of 2DNPC by proposing a novel scheme for fourth-harmonic generation (FHG) in which the fundamental and fourth-harmonic (FH) waves are collinear. Our scheme also has the advantage that the conversion efficiency exceeds that of other schemes by a factor that reaches 4 at low intensities.

FHG has been the subject of many studies, all of which considered two parametric processes, $\omega + \omega = 2\omega$ and $2\omega + 2\omega = 4\omega$, and often required the use of either two different crystals or two different, consecutive QPM gratings mounted on a single substrate. More complicated FHG may occur in a single nonlinear crystal that supports simultaneous phase matching of the two processes, e.g., in QPM structures, in which simultaneous phase matching is possible if the refractive indices satisfy a specific relation.[6,7] Additionally, double phase matching can be achieved in 2DNPC for arbitrary refractive indices, but the main disadvantage of the schemes proposed so far is that the fundamental and the FH beams are noncollinear.[4] FHG in a single crystal was observed in lithium formiate[8] and $LiNbO_3$,[3,9] but the efficiency was low since only one of the processes was phase matched. In particular, Broderick *et al.*[3] used a $LiNbO_3$ 2DNPC with a hexagonal lattice and observed simultaneous second-harmonic (SH) generation, third-harmonic generation, and FHG driven by the fundamental wavelength $\lambda = 1553$ nm. Although the SH generation was phase matched, the generation of higher harmonics was not, and the conversion efficiency was thus low.

In the scheme that we suggest, the FH wave results from the simultaneous action of three phase-matched processes. Two of these processes lead to the generation of a pair of SH waves, and the third one to the generation of the FH wave by mixing of the two SH waves. This scheme is illustrated in Fig. 1(a). The fundamental wave, with wave vector $\mathbf{k}_1$, propagates along the x axis. The two SH waves, with wave vectors $\mathbf{k}_{2a}$ and $\mathbf{k}_{2b}$ ($k_{2a} = k_{2b} \equiv k_2$), make angles $\pm\theta$ with respect to the x axis [see Fig. 1(a)]. The interaction of the two SH waves leads to the generation of a FH wave with the wave vector $\mathbf{k}_4$ collinear with the fundamental wave. These processes thus take place in a single 2DNPC structure.

We take the reciprocal lattice basis vectors of 2DNPC to be $\mathbf{K}_a = (2\pi/d)(\cos\varphi, \sin\varphi)$ and $\mathbf{K}_b = (2\pi/d)(2\cos\varphi, 0)$. The vector $\mathbf{K}_a$ is used for phase matching of the process, leading to a SH wave that propagates at angle θ with the x axis [see Fig. 1(a)];

0146-9592/01/080539-03$15.00/0

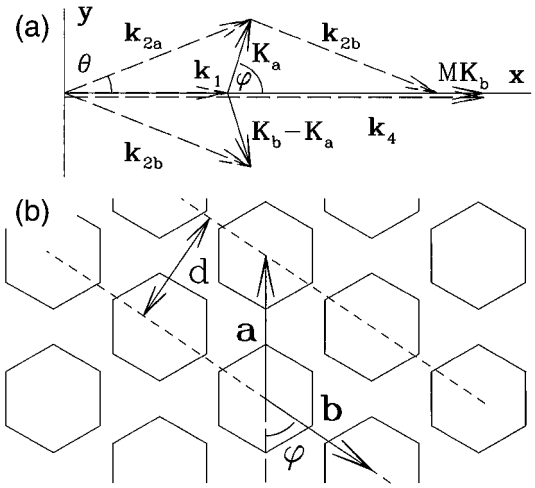

Fig. 1. (a) Schematic of the proposed frequency-conversion scheme. Reciprocal lattice vectors are indicated by dashed arrows; wave vectors, by solid arrows. (b) Associated real lattice for $LiTaO_3$ at 150 °C and $\lambda = 1.53$ μm.

$\mathbf{K}_b - \mathbf{K}_a = (2\pi/d)(\cos\varphi, -\sin\varphi)$ leads to a SH wave that propagates at $-\theta$ with the x axis. Finally, the reciprocal lattice vector $M\mathbf{K}_b$, where M is an integer that is yet to be determined, phase matches the process that generates the FH from the two SH beams. Because of the symmetry of the structure, the FH propagates parallel to the incident fundamental beam. With these definitions, we can write the phase-matching conditions as

$$2k_1 + (2\pi/d)\cos\varphi = k_2\cos\theta\,, \qquad (1)$$

$$(2\pi/d)\sin\varphi = k_2\sin\theta\,, \qquad (2)$$

$$2k_2\cos\theta + (4\pi M/d)\cos\varphi = k_4\,, \qquad (3)$$

corresponding to phase matching of the x and y components of the SH generation process and the x components of the FHG process. Note that the y components of the FHG process are phase matched by symmetry. It is easy to see from Eqs. (1)–(3) that

$$\cos\theta = (n_4 + Mn_1)/[(M+1)n_2]\,, \qquad (4)$$

where n_1, n_2, and n_4 are the refractive indices of the host material at the fundamental, SH, and FH frequencies, respectively. Integer M is now chosen to be the smallest positive integer for which Eq. (4) can be satisfied for a real angle θ; i.e., M equals the smallest integer exceeding $(n_4 - n_1)/(n_2 - n_1)$. The result depends on the material that is used and on the temperature and the wavelengths that are chosen. It is further found that

$$d = \lambda_1/(2h)\,, \qquad \cos\varphi = (n_4 - n_1)/[(M+1)h]\,, \quad (5)$$

where $h = [{n_2}^2 - {n_1}^2 - 2n_1(n_4 - n_1)/(M+1)]^{1/2}$. If M is chosen following the procedure described above, then φ is real; hence the lattice provides enough flexibility to guarantee that the parameters can be found to satisfy all three phase-matching conditions simultaneously.

The basis vectors $\mathbf{a}$ and $\mathbf{b}$ of the two-dimensional lattice satisfy $\mathbf{a}.\mathbf{K}_a = 2\pi$, $\mathbf{b}.\mathbf{K}_a = 0$, $\mathbf{a}.\mathbf{K}_b = 0$, and $\mathbf{b}.\mathbf{K}_b = 2\pi$, leading to $\mathbf{a} = d(0, 1/\sin\varphi)$ and $\mathbf{b} = (d/2)(1/\cos\varphi, 1/\sin\varphi)$. We note that when $\varphi = 30°$ or $\varphi = 60°$ the lattice is hexagonal, whereas when $\varphi = 45°$ it is square. An example of such a lattice is given in Fig. 1(b), which is appropriate for $LiTaO_3$ at temperature $T = 150$ °C and a fundamental wavelength $\lambda = 1.53$ μm. For this case $n_1 = 2.1241$, $n_2 = 2.1630$, and $n_4 = 2.3146$,[10] so $M = 4$, $\theta = 1.56°$, $d = 11.25$ μm, and $\varphi = 55.91°$.

Until now, we have considered only the lattice parameters and not the content of the unit cell. Here we consider unit cells that contain a single hexagon in which $\chi^{(2)}$ is inverted with respect to the surroundings. Although the size and orientation of this hexagon do not affect the phase matching, in our procedure these parameters are chosen to optimize the efficiency of the FHG process. To understand this choice, recall that the amplitudes of the nonlinearity that enter the evolution equations [see Eqs. (6), below] are the spatial Fourier transform of the unit cell, evaluated at the relevant reciprocal lattice vectors, which here are $\mathbf{K}_a$ and $M\mathbf{K}_b$ (by symmetry, the result at $\mathbf{K}_a$ equals that at $\mathbf{K}_b - \mathbf{K}_a$); we denote these amplitudes f_1 and f_2, respectively. Since this aspect of our procedure is identical to those in conventional one-dimensional QPM structures,[11] we do not discuss it in detail. However, in the example here we chose the orientation shown in Fig. 1(b), with a distance between the hexagon's center and corners of 5.1 μm. In the other orientation that was considered, the hexagons are rotated by 30° with respect to that shown in Fig. 1(b).

A key feature of our scheme is that two distinct SH waves are generated. Ignoring depletion, this leads to a total SH amplitude that is twice that in other schemes. The FH amplitude thus also doubles, so the efficiency is four times higher. To evaluate this and other features of our scheme, we model it in a cw approximation, using plane waves in which losses and spatial walk-off effects are ignored and perfect phase matching is assumed. Denoting, then, the wave amplitudes of the fundamental, the SH propagating at $+\theta$ and $-\theta$ with respect to the x axis, and the FH by A, S_a, S_b, and H, respectively, we can write the evolution equations as

$$\frac{\partial A}{\partial x} = -i\sigma_1 S_a A^* - i\sigma_1 S_b A^*, \qquad (6a)$$

$$\frac{\partial S_{a,b}}{\partial x} = -i\sigma_1 A^2 - i\sigma_2 H {S_{b,a}}^*, \qquad (6b)$$

$$\frac{\partial H}{\partial x} = -i2\sigma_2 S_a S_b\,. \qquad (6c)$$

Here $\sigma_1 = 2\pi f_1 d_{33}/(\lambda_1 n_1)$ and $\sigma_2 = 4\pi f_2 d_{33}/(\lambda_1 n_2)$ are the coefficients characterizing the two conversion

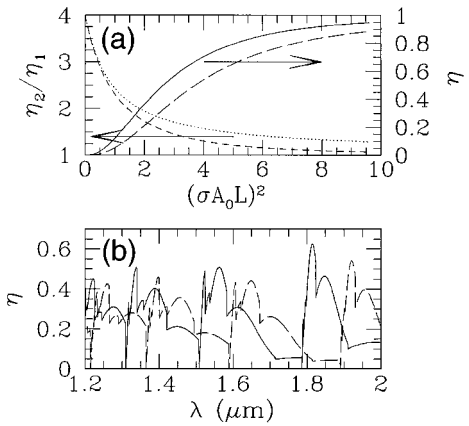

Fig. 2. (a) Right, FH conversion efficiency versus dimensionless fundamental intensity for the two-channel method (solid curve) and the single-channel method (long-dashed curve). Left, advantage of the two-channel method compared with the conventional single-channel geometry, according to Eq. (7) (dotted curve) and numerical calculations (short-dashed curve). (b) FH conversion efficiency versus wavelength for $LiNbO_3$ (dashed curve) and $LiTaO_3$ (solid curve); the other parameters are given in the text.

processes, $\omega + \omega = 2\omega$ and $2\omega + 2\omega = 4\omega$, respectively, and d_{33} is the relevant element of the $\chi^{(2)}$ tensor of the host material. System (6) can be solved at three distinct levels: (a) In one analytical solution, it is assumed that neither the fundamental wave that is due to SH generation nor the SH wave that is due to FHG is depleted. We then find that efficiency $\eta_{\mathrm{FHG}} = 4{\sigma_2}^2{\sigma_1}^4{A_0}^6L^6/9$, where A_0 is the input amplitude and L is the sample length. This is indeed four times larger than the corresponding result for the single-channel FHG method. (b) In the other analytical solution, only the depletion of the SH waves due to FHG is neglected. It is then found that

$$\eta_{\mathrm{FHG}} = {\sigma_2}^2\left[A_0L - \frac{1}{\sqrt{2}\,\sigma_1}\tanh(\sqrt{2}\,\sigma_1 A_0 L)\right]^2, \quad (7)$$

which reduces to result (a) for $\sigma_1 A_0 L \ll 1$. The result for the single-channel case can be obtained from Eq. (7) by replacement of $\sqrt{2}\,\sigma_1$ with σ_1. (c) Finally, we can solve Eqs. (6) numerically, which accounts for all depletion processes. In Fig. 2(a), on the right-hand scale, we compare the numerically calculated efficiencies of two- and single-channel FHG. We also show the FH efficiency ratio η_2/η_1 of these two schemes, which is found from Eq. (7) and numerical calculations. Although the advantage of the two-channel method disappears at high intensities, for low and intermediate intensities this method is clearly superior. We point out that such an advantage is possible only in 2DNPC structures.

In Fig. 2(b) we show the FHG efficiency of a 1-cm-long 2DNPC made from $LiNbO_3$ (dashed curve; input intensity, 60 MW/cm^2) and $LiTaO_3$ (solid curve; input intensity, 200 MW/cm^2) at 150 °C, calculated according to Eq. (7). At each wavelength we optimized the efficiency by maximizing the product ${f_1}^2 f_2$ by appropriately choosing the size and orientation of the hexagon in the unit cell. Although such optimization is critical for the high efficiencies that can be achieved with our method, we note that maximizing the product $f_1 f_2$ gives similar results. Note that for $LiNbO_3$ high efficiencies can be obtained for lower input intensities than in $LiTaO_3$ because the effective second-order nonlinearity is two times larger in $LiNbO_3$. The efficiency curves in Fig. 2(b) can be shifted by a change in temperature. We did not consider the wavelength dependence of the conversion efficiency for a fixed structure.

In conclusion, we have proposed and analyzed a novel scheme for efficient single-crystal FHG based on a 2DNPC structure. The method, suitable parameters for which are guaranteed to exist for any dispersion, ensures collinear propagation of the fundamental and the FH wave and is more efficient than conventional schemes. The high efficiency of the scheme presented is due to the simultaneous generation of two SH waves, a feature that is unique to 2DNPC. Although we illustrated our scheme with examples in $LiNbO_3$ and $LiTaO_3$, it can be applied to any host material that can be poled.

This work was partially supported by the Australian Research Council and the Performance and Planning Fund of the Australian National University. Y. S. Kivshar thanks M. Fejer for useful comments. M. de Sterke's e-mail address is desterke@Physics.usyd.edu.au.

References

1. See, e.g., S. Fan and J. D. Joannopoulos, Opt. Photon. News **11**(10), 28 (2000).
2. V. Berger, Phys. Rev. Lett. **81,** 4136 (1998).
3. N. G. R. Broderick, G. W. Ross, H. L. Offerhaus, D. J. Richardson, and D. C. Hanna, Phys. Rev. Lett. **70,** 4345 (2000).
4. S. Saltiel and Yu. S. Kivshar, Opt. Lett. **25,** 1204 (2000).
5. A. Chowdhury, S. C. Hagness, and L. McCaughan, Opt. Lett. **25,** 832 (2000).
6. O. Pfister, J. S. Wells, L. Hollberg, L. Zink, D. A. Van Baak, M. D. Levenson, and W. R. Bosenberg, Opt. Lett. **22,** 1211 (1997).
7. A. Sukhorukov, T. J. Alexander, Yu. S. Kivshar, and S. Saltiel, Phys. Lett. A **281,** 34 (2001).
8. S. A. Akhmanov, A. N. Dubovik, S. M. Saltiel, I. V. Tomov, and V. G. Tunkin, Pis'ma Zh. Eksp. Teor. Fiz. **20,** 264 (1974) [JETP Lett. **20,** 117 (1974)].
9. B. A. Hooper, D. J. Gauthier, and J. M. J. Madey, Appl. Opt. **33,** 6980 (1994).
10. J. P. Meyn and M. M. Fejer, Opt. Lett. **22,** 214 (1997).
11. M. M. Fejer, G. A. Magel, D. H. Jundt, and R. L. Bayer, IEEE J. Quantum Electron. **28,** 2631 (1992).